IEEE Access
Multidisciplinary ⋮ Rapid Review ⋮ Open Access Journal

Received 26 June 2023, accepted 18 July 2023, date of publication 26 July 2023, date of current version 2 August 2023.

Digital Object Identifier 10.1109/ACCESS.2023.3298972

RESEARCH ARTICLE

An Intelligent Inversion Method for Azimuth Electromagnetic Logging While Drilling Measurements

ZHENGMING KANG[1], YI ZHANG[2], HAOJIE QIN[1], WEI GAN[1], AND GANG CHEN[2]
[1]School of Electronic Engineering, Xi'an Shiyou University, Xi'an 710065, China
[2]Xi'an Research Institute, China Coal Technology and Engineering Group Corporation, Xi'an 710077, China

Corresponding author: Haojie Qin (3317574014@qq.com)

This work was supported in part by the Scientific Research Program funded by the Education Department of Shaanxi Provincial Government under Grant 22JY053, in part by the Shaanxi Province Key Research and Development Program under Grant 2023-YBGY-111, in part by the China Postdoctoral Science Foundation Program under Grant 2022M711442, in part by Shaanxi Province Qin Chuangyuan Cited High-Level Innovation and Entrepreneurship Talent Project under Grant QCYRCXM-2022-260, and in part by Xi'an Research Institute Co. Ltd. Science and Technology Innovation Fund Program under Grant 2023XAYJS01.

ABSTRACT Azimuth electromagnetic (EM) Logging While Drilling (LWD) tools play an important role in geological steering and reservoir evaluation. Its measuring response is amplitude ratio (ATT) and phase difference (PS), which can't directly reflect formation information. To obtain direct formation information such as resistivity and formation boundary, accurate and efficient inversion method is essential. However, the existing inversion methods (i.e., iterative method) have some problems, such as slow computation speed, dependence on initial value selection and easy to be trapped by local minimum. Therefore, this paper proposes an intelligent inversion method for azimuthal EM LWD measurements based on the U-net deep learning network framework. Firstly, an efficient analytical solution is used to generate amounts of EM LWD data. Those samples are divided into training and test sets in a 9:1 ratio, which are used for training and testing of the network, respectively. Then, the network parameters are constantly adjusted during training to ensure its inversion performance. Finally, the trained network is utilized to invert the samples of the test sets, and the inversion results are compared with the forward formation model. The study's results demonstrate that the network is capable of efficiently and precisely inverting both isotropic and anisotropic formations, with a single sample being inverted less than 0.05 seconds. Its noise layer parameters can be improved to successfully invert noisy data, leading to good robustness. In addition, the network has good applicability for the inversion of complex formations. These consequences highlight the significant potential of this method in azimuthal EM LWD inversion applications.

INDEX TERMS Intelligent inversion, azimuth EM LWD, resistivity, formation boundary.

I. INTRODUCTION

In recent years, the azimuthal EM LWD tool has been widely used in geosteering and reservoir evaluation [1], since it can provide azimuth information of formation boundary [2], [3]. Its measurement signals are ATT and PS. They can't directly reflect the information of resistivity and the distance between the tool and formation boundary. It is necessary to obtain the formation resistivity and interface position by inversion methods. Presently, the inversion methods of azimuthal EM LWD consist of gradient algorithm and artificial intelligence algorithm.

Gradient algorithms use gradient information to search for the descending direction to obtain the solution of the least squares problem [4], [5], and the more commonly used are the Born inversion method and the Gauss-Newton (GN) method. Born method can be used for inversion calculation of low-frequency EM field [6], but the iteration speed is slow, and the convergence of high-resistivity contrast model is poor [7]. The degenerated Born iterative

The associate editor coordinating the review of this manuscript and approving it for publication was Sandra Costanzo.

method (DBIM) was proposed by Chew and improved by many scholars [8], [9]. It can be used to analyze the EM field problems in 2D or 3D high-resistivity contrast models [10], [11]. Its convergence rate is faster than that of Born method, but the calculation amount of DBIM is much larger than that of Born method [12]. Compared with GN and other nonlinear convergence algorithms, the Born method is a linear convergence algorithm, and its convergence speed is slow. In fact, the inversion of azimuthal EM LWD requires high real-time performance, so the applicability of Born method is limited.

GN method proposed by Gauss [13] is widely used in inverting the azimuthal EM LWD data [14], [15]. It directly minimizes the resulting quadratic function and avoids evaluating the second derivative of the regression function. The convergence rate is significantly better than the linear convergence rate [16]. However, GN method has a high requirement for selecting initial value, and an improper initial value may cause method failure or local minimum.

The use of deep learning in the inversion of azimuthal EM LWD measurements has become increasingly prevalent in recent years, largely due to advancements in computer performance [17], [18], [19], [20]. Many scholars use different deep learning networks to invert the data of EM measurement. Shahriari et al. used deep learning method to invert logging data in anisotropic formation, but the inversion results were very different from the real formation information, so it couldn't be directly used for interpretation of logging data in anisotropic formation and could only be used as a reference before inversion [21]. Fan et al. used LSTM network to invert geological parameters such as formation boundary and resistivity, while also estimating the uncertainty of inversion results. However, they didn't verify the inversion of noise data [22]. Hu et al. combined deep neural networks (DNNs) with traditional inversion flow and improved inversion results by using multi-physical data iteration [23]. Zhu et al. used the three-layer formation model to invert parameters such as resistivity and layer thickness in anisotropic formations and obtained relatively accurate inversion results. However, due to the simple network architecture, complex and diverse logging response could not be processed [24]. Noh et al. established an inversion flow of the three-layer formation model based on the ResNet network to invert the formation resistivity distribution and fault state in the presence of faults [25], [26]. Jin et al. developed an inversion network for azimuthal EM LWD measurements using a combination of data-driven and physically driven models. However, the formation model used in their study was limited in its simplicity and did not account for the network's applicability to anisotropic formations [27].

Compared to shallow neural network with limited computational accuracy, convolutional neural networks have more hidden layers and can extract richer input data information with higher computational accuracy [28]. The published results show that the trained convolutional neural network could invert azimuthal EM LWD measurements quickly. This is a significant improvement in comparison to traditional methods, which are known to have slower calculation speeds. As a result, this approach has the potential to address the problem of slow calculations in this field. However, the application of convolutional neural network in azimuthal EM LWD is still in its infancy. To apply it to actual data processing, it still needs further research work.

Therefore, we developed an inversion flow for azimuthal EM LWD measurements using a U-net convolutional neural network. The flow was analyzed to determine the role of each component and the training parameters of the network were optimized. The trained network demonstrated high accuracy and efficiency in inverting azimuthal EM LWD measurements, while also exhibits good robustness.

II. DATA INVERSION FLOW

This paper presents an inversion flow for azimuthal electromagnetic measurements, utilizing a convolutional neural network, as shown in Figure 1. The flow starts with establishing a formation model to calculate the forward sample (Figure 1a). The data obtained from a single sample is represented as a 2D image comprising 72 curves, each curve containing 128 sampling points (Figure 1b). Then, a large number of 2D image samples are used to train the convolutional neural network (Figure 1c). Once trained, the network can extract features from azimuthal EM LWD measurements and predict new data as depicted in Figure 1d.

A. FORWARD SAMPLES GENERATION

1) FORWARD MODELLING

Convolutional neural network inversion requires a significant number of samples. However, the numerical method that is appropriate for 3D problems has a slow computation speed, which fails to meet the requirements of making a large number of samples. In cases where the tool size is relatively small compared to the formation fluctuation, the 3D model can be approximated as the 2D geological model, as shown in Figure 2a. The 2D geological model can be simplified as a horizontal layered formation when the formation undulation changes little in comparison to the tool scale, as depicted in Figure 2b. At this point, the analytical method can be used to calculate the solution of the EM field. The generalized reflection coefficient method [29] is utilized in this paper to generate the samples of the azimuthal EM LWD measurements.

2) TOOL PARAMETER

In our study, we utilized Schlumberger's PeriScope as the tool for forward calculation. The structure of the tool is depicted in Figure 3. It comprises axial, inclined, and radial coil systems that can effectively measure resistivity and geological signals. Table 1 lists the combination of space (s), frequency (f), and coil system. It has a total of 72 ATT and PS measurement signals at the same sampling point.

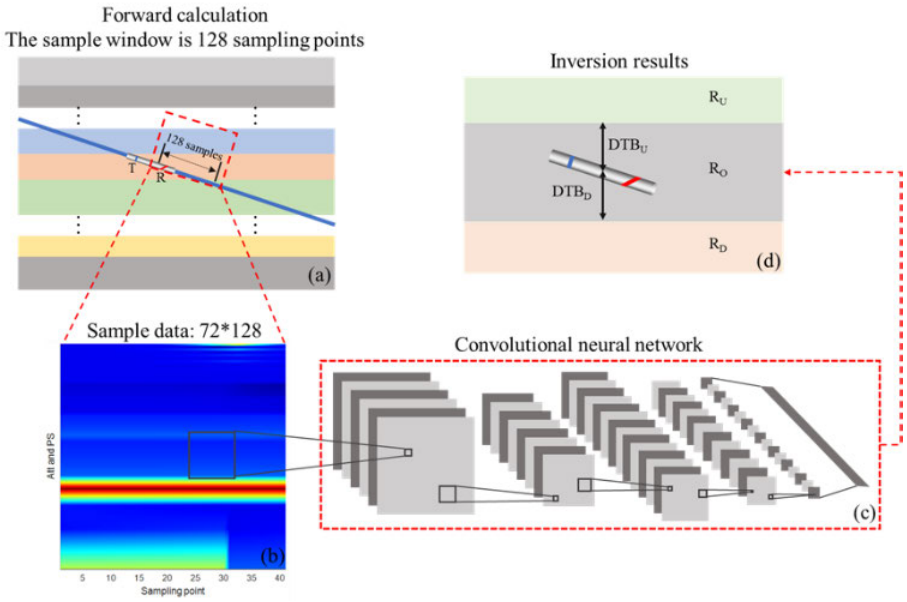

FIGURE 1. Inversion flow of the azimuthal EM LWD measurements.

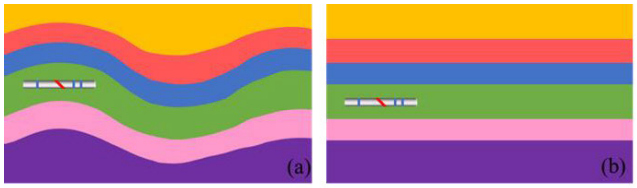

FIGURE 2. Geological model approximation.

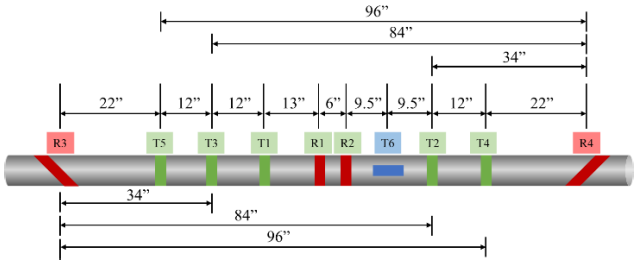

FIGURE 3. Structure of PeriScope azimuthal EM LWD tool.

TABLE 1. The coil array of periScope.

Coil array	Axial coil	Inclined coil	Radial coil
f/MHz	0.4, 2	0.1, 0.4, 2.0	0.1, 0.4
S/in	16, 22, 28, 34, 40	22, 34, 84, 96	43.5, 74.5
Symmetry	No	Yes	No
Total (ATT, PS)	20	48	4

3) SAMPLE CALCULATION METHOD

This paper utilizes the propagation coefficient matrix method to compute the response of a 2D horizontal stratified formation model, as illustrated in Figure 2b. Unlike the numerical mode match (NMM) method, this approach eliminates the need to solve 2N equations with N layer interfaces simultaneously, so it has a faster calculation speed.

The propagation of EM in homogeneous medium satisfies Maxwell's equations in differential form:

$$\begin{cases} \nabla \times \boldsymbol{H} = \boldsymbol{J} + \dfrac{\partial \boldsymbol{D}}{\partial t} \\ \nabla \times \boldsymbol{E} = -\dfrac{\partial \boldsymbol{B}}{\partial t} \\ \nabla \cdot \boldsymbol{B} = 0 \\ \nabla \cdot \boldsymbol{D} = \rho \end{cases} \tag{1}$$

where $\boldsymbol{H}$ is magnetic field strength. $\boldsymbol{J}$ signifies conducted current density. $\boldsymbol{E}$ denotes electric field intensity. $\boldsymbol{B}$ represents magnetic induction intensity. $\boldsymbol{D}$ indicates electric displacement vector. ρ signifies the charge density.

In the context of azimuthal EM LWD method, the transmitting coil can be treated as a magnetic dipole source. The resulting time-harmonic field can be described by the Maxwell equations:

$$\begin{cases} \nabla \times \boldsymbol{H} = \sigma \cdot \boldsymbol{E} \\ \nabla \times \boldsymbol{E} = i\omega \boldsymbol{B} \\ \boldsymbol{B} = \mu_0 \boldsymbol{H} + \mu_0 \boldsymbol{M}_S \end{cases} \tag{2}$$

$$\boldsymbol{\sigma} = \begin{bmatrix} \sigma_h & 0 & 0 \\ 0 & \sigma_h & 0 \\ 0 & 0 & \sigma_v \end{bmatrix} \tag{3}$$

where σ_h denotes the horizontal conductivity. σ_v indicates the vertical conductivity. ω is the angular frequency. μ_0 signifies magnetic permeability in vacuum. $\boldsymbol{M}_S$ represents the applied magnetics current.

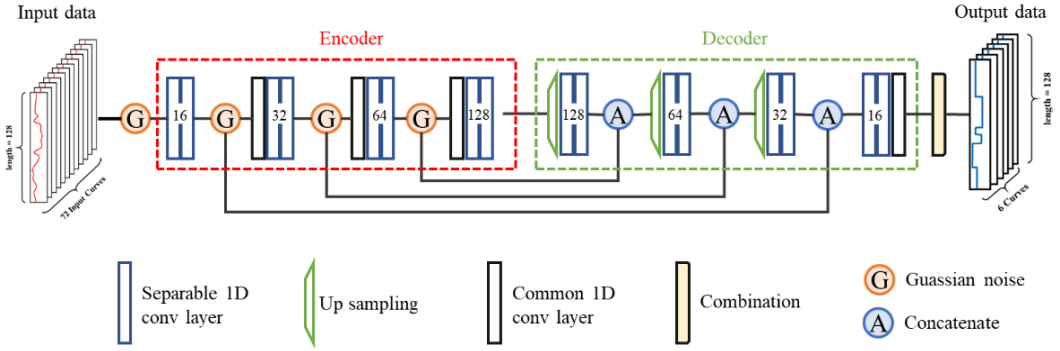

FIGURE 4. Inversion network model of azimuthal EM LWD.

The Hertz potential theory is used in the derivation, and the Hertz vector potential and scalar potential satisfy:

$$\begin{cases} \boldsymbol{\sigma} \cdot \boldsymbol{E} = i\omega\mu_0\sigma_h \nabla \times \boldsymbol{\pi} \\ \boldsymbol{H} = i\omega\mu_0\sigma_h \boldsymbol{\pi} + \nabla \boldsymbol{\Psi} \\ \nabla \cdot (\boldsymbol{\sigma} \cdot \boldsymbol{\pi}) = \sigma_v \boldsymbol{\Psi} \end{cases} \tag{4}$$

By substituting equation (4) into equation (3), the expression of magnetic dipole source in uniformly anisotropic media can be obtained, and it can be transformed into the cylindrical coordinate system.

$$\begin{cases} E_z = -\dfrac{1}{4\pi}\left(M_x \sin\alpha - M_y \cos\alpha\right) \\ \displaystyle\int_0^\infty \omega\mu\lambda k_\rho^2 i \frac{J_1\left(k_\rho\rho\right)}{k_{v,z}} e^{i\lambda|z|k_{v,z}} k_\rho dk_\rho \\ H_z = \dfrac{1}{4\pi}\left(M_x \cos\alpha + M_y \sin\alpha\right) \\ \displaystyle\int_0^\infty k_\rho^2 \frac{\partial|z|}{\partial z} J_1\left(k_\rho\rho\right) e^{i|z|k_{v,z}} dk_\rho + \\ \dfrac{M_z}{4\pi}\displaystyle\int_0^\infty ik_\rho^3 \frac{J_0\left(k_\rho\rho\right)}{k_{h,z}} e^{i|z|k_{h,z}} dk_\rho \end{cases} \tag{5}$$

In equation (5), M_x, M_y and M_z are the components of magnetic moments in the x, y and z direction. $\lambda^2 = \sigma_h/\sigma_v$ indicates the anisotropy coefficient. k_ρ denotes the integral variable. J_1 represents first-order Bessel function. α indicates the well inclination angle. μ is the permeability. h indicates a horizontal magnetic dipole. z and z_0 are the ordinate of the receiving point and the transmitting source position respectively. v indicates a vertical magnetic dipole.

Chew's theory proposes that in a 2D anisotropic formation model, it is only necessary to calculate the vertical components of the EM field for each layer. The horizontal component can then be obtained, allowing for the solution of the entire EM field. In cylindrical coordinate system, the vertical component of EM field in horizontal layered model is calculated by the following recursive formula [29]:

$$\boldsymbol{E}_{n,z} = -\frac{1}{4\pi}\left(M_x \sin\alpha - M_y \cos\alpha\right) \omega\mu\lambda_n \frac{k_\rho^2}{k_{n,v,z}} J_1\left(k_\rho\rho\right) F_n^{TM,h} \tag{6}$$

$$\boldsymbol{H}_{n,z} = \frac{1}{4\pi}\left(M_x \cos\alpha + M_y \sin\alpha\right) k_\rho^2 J_1\left(k_\rho\rho\right) F_n^{TM,h} + \frac{M_z}{4\pi}\frac{ik_\rho^3}{k_{n,h,z}}\left(k_\rho\rho\right) F_n^{TM,v} \tag{7}$$

where $\boldsymbol{E}_{n,z}$ denotes the vertical component of electric field of the n-th layer. $\boldsymbol{H}_{n,z}$ represents the magnetic field component of the n-th layer medium. F_n signifies the propagation coefficient of the nth layer. $k_{n,v,z}$ denotes the vertical component of the wave number of the n-th layer medium. The superscript TM is the z component of the TM wave.

The expression for the ρ and φ components of the EM field is given by the following equation:

$$\begin{bmatrix} \boldsymbol{E}_\rho \\ \boldsymbol{E}_\varphi \end{bmatrix} = \frac{1}{\lambda^2 k_\rho^2}\begin{bmatrix} 0 & -1 \\ 1 & 0 \end{bmatrix}\begin{bmatrix} \frac{1}{\rho}\frac{\partial^2}{\partial z \partial \varphi} \\ -\frac{\partial^2}{\partial z \partial \rho} \end{bmatrix}\boldsymbol{E}_z + \frac{i\omega\mu}{k_\rho^2}\begin{bmatrix} \frac{1}{\rho}\frac{\partial}{\partial \varphi} \\ -\frac{\partial}{\partial \rho} \end{bmatrix}\boldsymbol{H}_z \tag{8}$$

$$\begin{bmatrix} \boldsymbol{H}_\rho \\ \boldsymbol{H}_\varphi \end{bmatrix} = \frac{1}{k_\rho^2}\begin{bmatrix} 0 & -1 \\ 1 & 0 \end{bmatrix}\begin{bmatrix} \frac{1}{\rho}\frac{\partial^2}{\partial z \partial \varphi} \\ -\frac{\partial^2}{\partial z \partial \rho} \end{bmatrix}\boldsymbol{H}_z + \frac{\sigma_h}{\lambda^2 k_\rho^2}\begin{bmatrix} \frac{1}{\rho}\frac{\partial}{\partial \varphi} \\ -\frac{\partial}{\partial \rho} \end{bmatrix}\boldsymbol{E}_z \tag{9}$$

The vertical component of EM field in each layer of horizontal layered formation model can be obtained by equation (8) and equation (9), and then the solution to the whole EM field can be obtained.

After obtaining the EM field component, the voltage on the receiving coil is calculated and converted into ATT and PS by equation (10) and equation (11):

$$\mathrm{Att} = 20\lg\frac{\sqrt{[\mathrm{Re}(V_{R1})]^2 + [\mathrm{Im}(V_{R1})]^2}}{\sqrt{[\mathrm{Re}(V_{R2})]^2 + [\mathrm{Im}(V_{R2})]^2}} \tag{10}$$

$$PS = \arctan\frac{\mathrm{Im}(V_{R1})}{\mathrm{Re}(V_{R1})} - \arctan\frac{\mathrm{Im}(V_{R2})}{\mathrm{Re}(V_{R2})} \tag{11}$$

where V_{R1} denotes the voltage signal received near the receiving coil. V_{R2} indicates the voltage signal received by the far receiver coil. Re and Im are the real part and imaginary part of V respectively.

The range of formation resistivity was set to 0.1 to 100 Ω·m, which is the typical range for oil reservoir resistivity. The formation thickness varies from 0.1 m to 8 m.

After performing the above calculation, 72 logging response curves can be obtained for each set of formation parameters. In this paper, 240,000 samples were generated by randomly selecting values of the formation parameters. These samples are further divided into 120,000 isotropic samples and 120,000 anisotropic samples.

B. U-NET CONVOLUTIONAL NEURAL NETWORK MODEL

In the inversion flow illustrated in Figure 1c, a U-net convolutional neural network is utilized to establish the inversion framework. The network employs an encoder-decoder structure, as shown in Figure 4. In the encoder section, the network utilizes multiple sets of depth separable convolutional layers and conventional convolutional layers to transform 72 responses of azimuthal EM LWD into several feature vectors, also known as hidden variables. Then these feature vectors are scaled and transformed into 6 one-dimensional sequences of the same size as the resistivity profile using the decoder part consisting of the upper sampling layer and the deconvolution layer. In this way, 72 measured responses were translated into formation parameters at the current point. Referring to previous practical experience [31]. We also add four Gaussian Noise Layers (0.01) [32] between these four separable 1D convolutional layers, which can prevent network learning from over-fitting and improve the robustness of the network.

III. NETWORK TRAINING

The performance of the network is influenced by the learning rate and batch size. A large learning rate can cause the loss function to oscillate and fail to converge, while a small learning rate will lead slow convergence or the loss function getting stuck in a local minimum. Increasing the batch size can lead a more accurate direction of decline and smaller loss shock within a certain range. To optimize the training parameters of the network, we experimented with different learning rates (0.01, 0.001, 0.0001, 0.00001) and batch sizes (64, 100, 128, 256). Table 2 records the loss errors of the network under different training parameters. The combination of all possibilities was explored. The network achieved the minimum average loss with a learning rate of 0.001 and a batch size of 100.

TABLE 2. Loss function values for different batch sizes and learning rates.

LR/BS	64	100	128	256
0.01	0.1939	0.1934	0.1962	0.0061
0.001	0.0041	0.0036	0.0043	0.0042
0.0001	0.0043	0.0046	0.0048	0.0049
0.00001	0.0071	0.0082	0.0076	0.0099

The paper specifies that the optimization algorithm used for training is the Adaptive Moment Estimation (Adam) optimizer, and the network loss function is the Mean Square Error (MSE). The network training error is a function of the weight $\boldsymbol{W}$, and the weight update formula is:

$$W_{i+1} = W_i - \eta \frac{\partial Loss}{\partial W} \tag{12}$$

where i denotes the number of iterations. W_i indicates the i-th learning weight. η signifies learning rate (LR). Loss represents the MSE under the current iteration number.

After determining the network parameters, the number of iterations was set to 400. The error changes during the training process were illustrated in Figure 5. It shows that the error no longer decreased significantly with the increasing number of epochs after 100 iterations. It indicates that the network has reached convergence. Furthermore, continuous training of the network does not cause an increase in error, indicating that the network does not exhibit overfitting even after sufficient training. Each training process takes approximately seven hours using an Nvidia GTX machine equipped with Intel i9-9900K CPU and a Nvidia GeForce RTX 2080 Ti GPU.

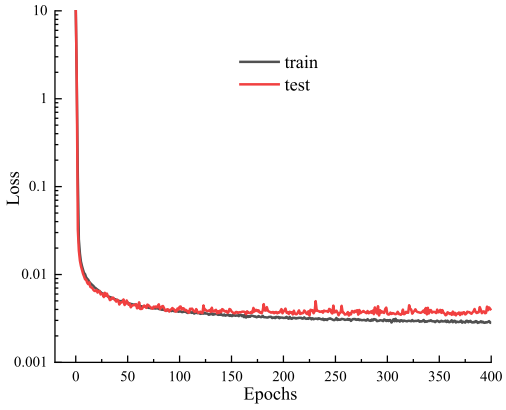

FIGURE 5. Change of MSE during training.

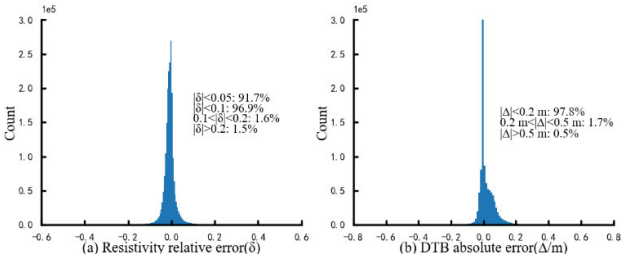

FIGURE 6. Error statistical results of isotropic model inversion.

IV. ANALYSIS OF INVERSION RESULTS

A. ISOTROPIC DATA INVERSION

The trained network was applied to a test set of 4000 isotropic samples, each with 128 sampling points. It had a total of 4000*128 sampling points. We counted the relative error of resistivity and the absolute error of the depth to boundary (DTB) at each sampling point and presented their distribution patterns in Figure 6. The results showed that in all sampling points, the relative error of resistivity was less than 10%,

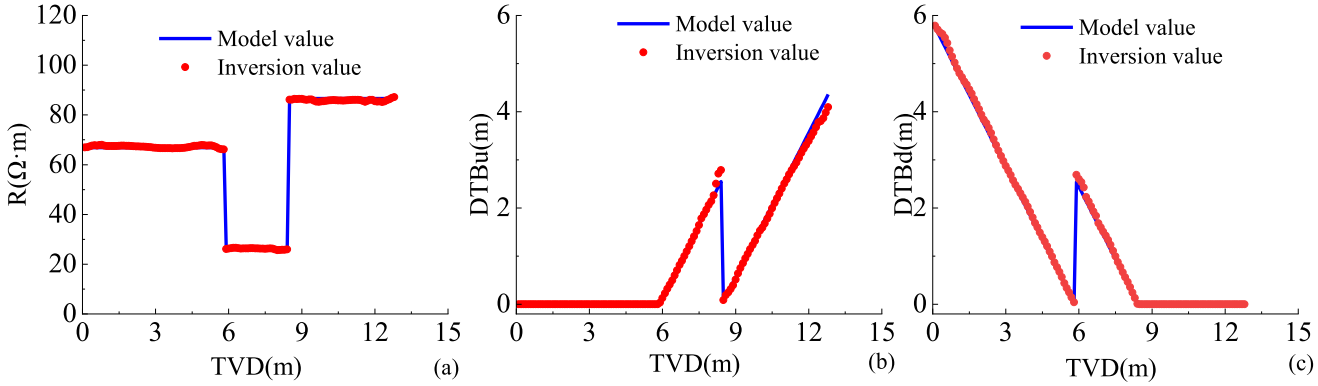

FIGURE 7. Inversion results of three-layers model.

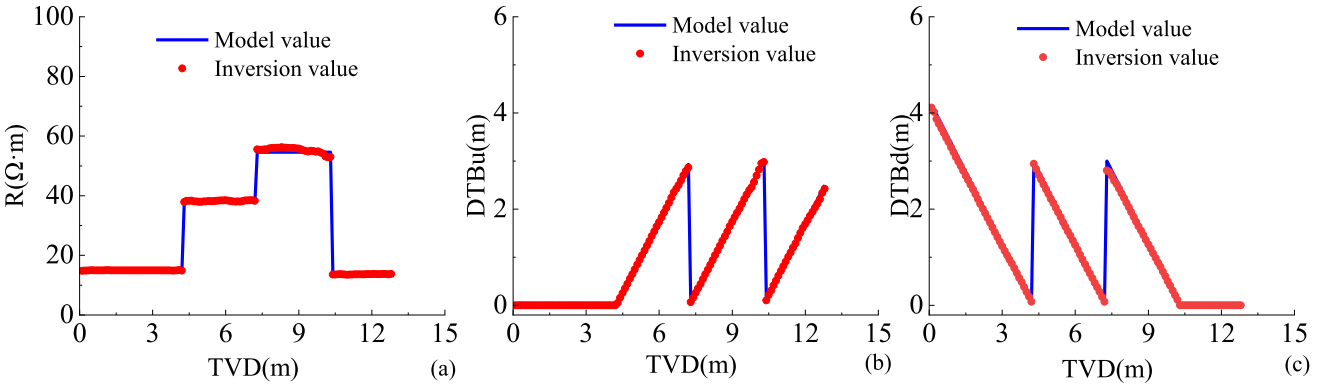

FIGURE 8. Inversion results of four-layers model.

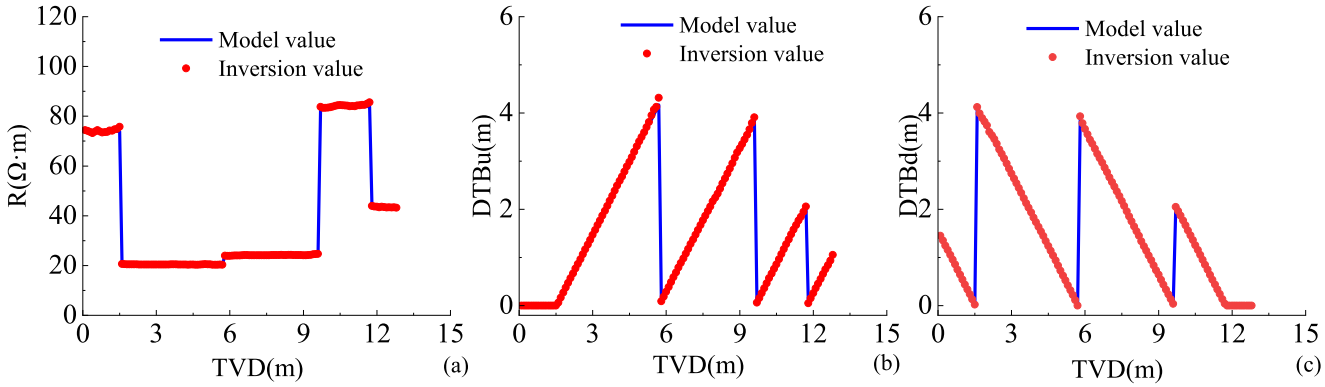

FIGURE 9. Inversion results of five-layers model.

occupying 96.9% of the points, and the absolute error of DTB was less than 0.2m, occupying 97.8% of the points. These results indicate that the network can effectively invert isotropic samples with high precision.

To ensure the accuracy and reliability of the inversion results, we randomly select one formation sample from three, four, and five-layer samples. We then compare the difference between the forward formation model and the inversion results, as shown in Figure 7 to Figure 9. In Figure 7a, the abrupt change in resistivity indicates the location of the formation boundary. At this point, the value of DTBu is set to 0 and DTBd represents the thickness of the formation below the boundary. The similarity between the forward model values and inversion values suggests that the formation information obtained through inversion is highly consistent with the forward formation model. This indicates that the U-net network is an efficient method for inverting azimuthal EM LWD measurements.

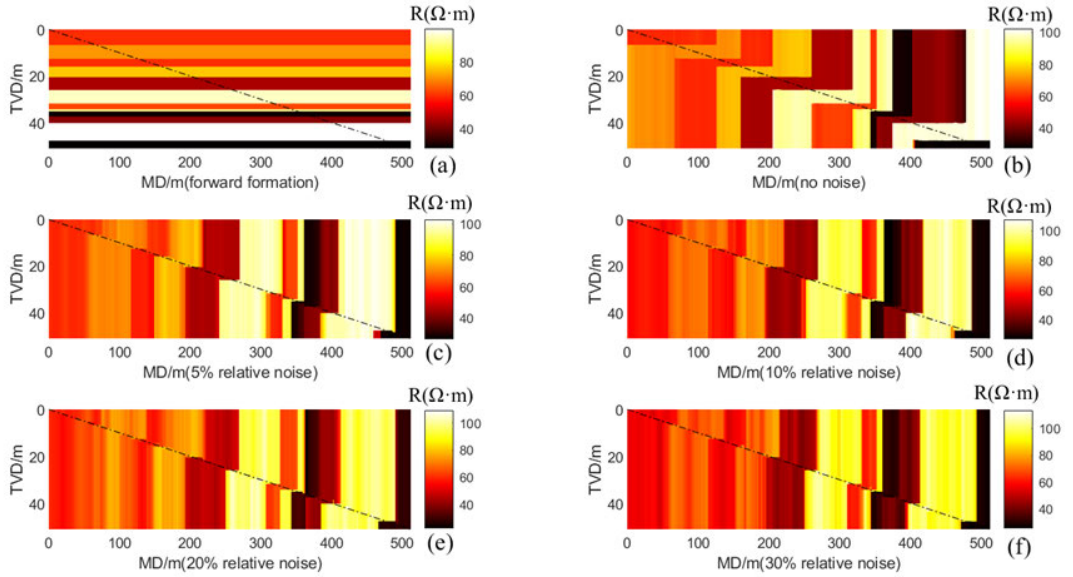

FIGURE 10. Inversion results of different noise data (Gaussian Noise Layers: 0.01).

The U-net network not only has high accuracy, but also has a fast inversion speed in inverting azimuthal EM LWD measurements. Test results reveal that the network can invert a single sample in less than 0.05 seconds on average, which is two orders of magnitude faster than the traditional inversion method [30].

To assess the robustness of the U-Net network, we conducted tests on data with varying levels of noise: 5%, 10%, 20%, and 30%. The forward formation model is shown in Figure 10a. Figure 10 (b, c, d, e, f) displays the 2D curtain map obtained through inversion under different noise intensities. The color of each pixel's represents the formation resistivity value, and the black dotted line indicates the LWD tool's path. In the absence of noise, the resistivity value experiences a sudden change when the tool crosses the formation interface and remains consistent with the forward formation. However, as the relative noise intensity increases, the accuracy of network rapidly declines, indicating poor robustness of the network.

To enhance the robustness of the network, the parameter value of the Gaussian noise layer was increased from 0.01 to 0.1. The network was then retrained using this new parameter and subsequently tested on the test set samples. The error distribution rule and the results of the robustness test are presented in Figure 11 and Figure 12 respectively. In 91.9% of the sampling points, the relative error of resistivity is less than 10%, while in 97.1% of the points, the absolute error of DTB is less than 0.2m. Enlarging the Gaussian noise layer parameters slightly decreases the inversion accuracy, but the logging data can still be inverted well. The network is able to perform a good inversion of data containing 10% relative noise, thereby improving its robustness significantly. According to the research,

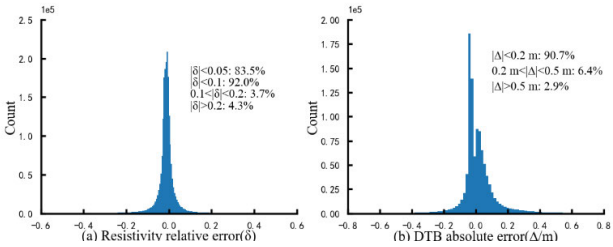

FIGURE 11. Error statistical results of isotropic model inversion.

expanding the parameters of the Gaussian noise layer can enhance the robustness of the network at a low cost to inversion accuracy. Therefore, during network training, it can obtain high robustness by increasing the parameters of the Gaussian noise layer as much as possible while meeting the requirements of accuracy.

B. ANISOTROPIC DATA INVERSION

To evaluate the effectiveness of the network on anisotropic formations, the horizontal stratified formation model as shown in Figure 1a was set to anisotropy, and 120,000 samples were generated. We trained and inverted the anisotropic sample data using the same network as described in Section IV-A. Figure 13 depicts the resistivity and formation boundary inversion curves of a randomly selected sample. The horizontal and vertical resistivity, as well as the formation boundary, all exhibit positive inversion effects. In Figure 14, the network inversion errors of 3000 test sample data were calculated, and it was found that the relative error of resistivity was less than 10% in 92.9% of the sampling points, while the absolute error of DTB was less than 0.2m in 90.7% of the points. Hence, the network is highly applicable to anisotropic data.

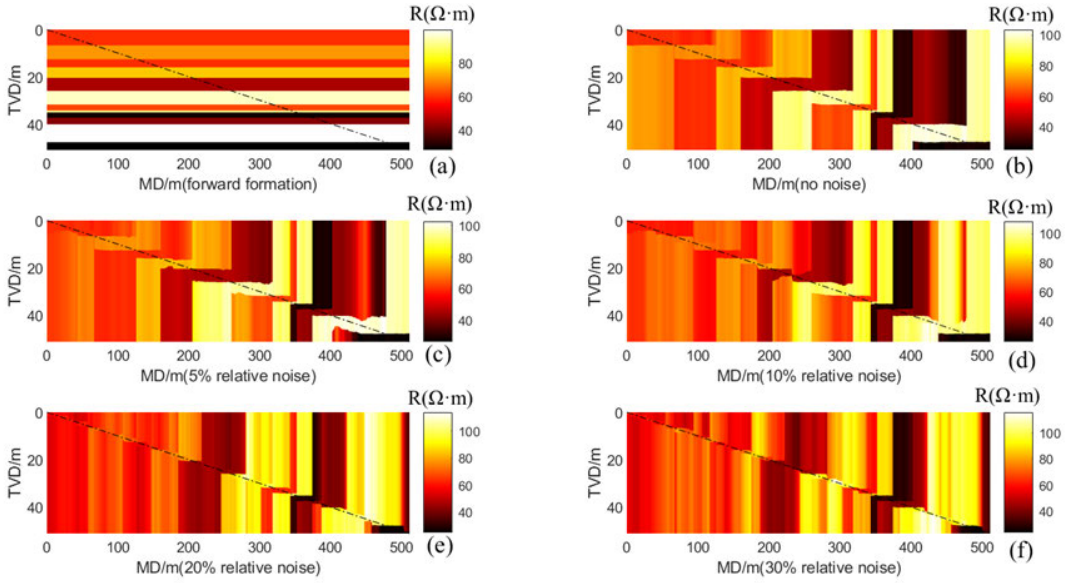

FIGURE 12. Inversion results of different noise data (Gaussian Noise Layers: 0.1).

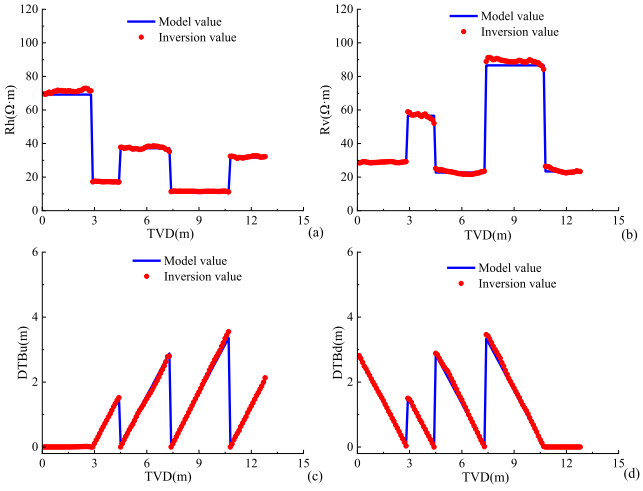

FIGURE 13. Inversion results of anisotropic model.

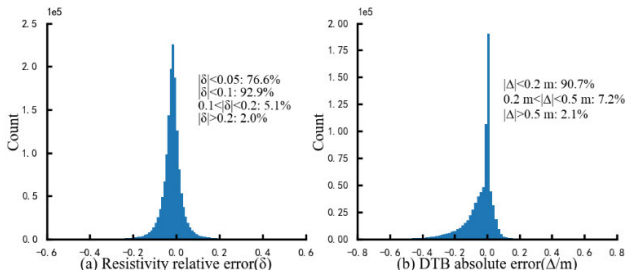

FIGURE 14. Error statistical results of anisotropic model inversion.

C. COMPLEX FORMATION INVERSION

To assess the effectiveness of the inversion network, we created a micro-undulating formation model consisting of five isotropic layers, as depicted in Figure 15a. The model accounts for changes in resistivity along the longitudinal direction of the formation, as well as heterogeneity in the transverse direction (The red line represents the path of the LWD tool). The EM response of the complex formation model is calculated by the finite element method and the 2D resistivity curtain by inverting is shown in Figure 15b. It indicates that the resistivity inversion outcomes are only marginally imprecise in the vicinity of the formation boundary. However, for the majority of measurement points, it accurately inverts the formation resistivity and determines the formation boundary position as the tool moves away from the formation boundary. Although our network is trained on horizontal formation samples, it is capable of accurately inverting micro-undulating formation models. This suggests that the network has strong applicability beyond its original training data.

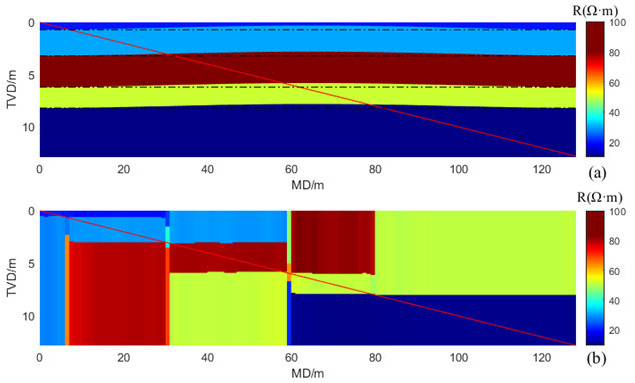

FIGURE 15. Inversion results of Complex formation model.

V. CONCLUSION

This paper proposes a new method for inverting azimuthal EM LWD measurements using U-net convolutional neural network. The study shows that the network can accurately invert isotropic and anisotropic horizontal stratified stratigraphic models. The method boasts an unmatched calculation speed compared to traditional inversion techniques, completing the inversion of a single sample in just 0.05 seconds. The study also reveals that the network's robustness can be improved by increasing the parameters of the Gaussian noise layer, albeit at a slight cost to inversion accuracy. According to the result, the trained network has a high inversion accuracy for data with noise levels below 10%.

The complex formation model is tested using the network, which shows high inversion accuracy and the inversion speed does not slow down with increasing complexity of the formation model. Therefore, the proposed method for inverting azimuthal EM LWD measurements is both accurate and efficient. The intelligent inversion method has significant potential for practical applications in LWD operations.

REFERENCES

[1] J. Zhou, H. Li, M. Rabinovich, and B. D. Arcy, "Interpretation of azimuthal propagation resistivity measurements: Modeling, inversion, application and discussion," in *Proc. SPWLA 57th Annu. Logging Symp.*, Reykjavik, Iceland, Jun. 2016, pp. 1–9.

[2] X.-C. Nie, N. Yuan, and C. R. Liu, "Simulation of LWD tool response using a fast integral equation method," *IEEE Trans. Geosci. Remote Sens.*, vol. 48, no. 1, pp. 72–81, Jan. 2010.

[3] H. O. Lee, F. L. Teixeira, L. E. S. Martin, and M. S. Bittar, "Numerical modeling of eccentered LWD borehole sensors in dipping and fully anisotropic earth formations," *IEEE Trans. Geosci. Remote Sens.*, vol. 50, no. 3, pp. 727–735, Mar. 2012.

[4] G. L. Wang, T. Barber, P. Wu, D. Allen, and A. Abubakar, "Fast inversion of triaxial induction data in dipping crossbedded formations," *Geophysics*, vol. 82, no. 2, pp. D31–D45, Mar. 2017.

[5] J. J. Moré, "The Levenberg–Marquardt algorithm: Implementation and theory," *Numer. Anal.*, vol. 630, pp. 105–116, Jan. 1978.

[6] Q. Zhou, "Audio-frequency electromagnetic tomography for reservoir evaluation," Ph.D. dissertation, Dept. Mater. Sci. Mineral Eng., Univ. California, CA, USA, Oct. 1989.

[7] D. G. Song, "The study on numerical stimulation and geosteering application of electromagnetic logging while drilling tools," Ph.D. dissertation, School Geophys. Geomat., China Univ. Geosci., Beijing, China, 2014.

[8] W. C. Chew and Q.-H. Liu, "Inversion of induction tool measurements using the distorted Born iterative method and CG-FFHT," *IEEE Trans. Geosci. Remote Sens.*, vol. 32, no. 4, pp. 878–884, Jul. 1994.

[9] H. Zheng, C. Wang, and E. Li, "Modification of enhanced distorted Born iterative method for the 2D inverse problem," *IET Microw., Antennas Propag.*, vol. 10, no. 10, pp. 1036–1042, Jul. 2016.

[10] T. J. Cui, W. C. Chew, A. A. Aydiner, and S. Chen, "Inverse scattering of two-dimensional dielectric objects buried in a lossy earth using the distorted Born iterative method," *IEEE Trans. Geosci. Remote Sens.*, vol. 39, no. 2, pp. 339–346, Feb. 2001.

[11] F. H. Li, Q. H. Liu, and L. P. Song, "Three-dimensional reconstruction of objects buried in layered media using Born and distorted Born iterative methods," *IEEE Geosci. Remote Sens. Lett.*, vol. 1, no. 2, pp. 107–111, Apr. 2004.

[12] L. H. Chen, J. G. Sun, Y. G. Wu, Z. R. Wang, L. G. Han, and J. W. Zhu, "Review of quasi-linear approximation in geophysical inversion," *Prog. Geophys.*, vol. 17, no. 3, pp. 464–472, Mar. 2022.

[13] C. Gauss, *Theory of the Motion of the Heavenly Bodies Moving about the Sun in Conic Sections*. Mineola, NY, USA: Dover, 1809.

[14] G.-L. Xing, M.-L. Zhang, M.-F. Liu, and S.-D. Yang, "An inversion method on formation dielectric constant and resistivity by using high frequency electromagnetic wave logging," *Chin. J. Geophys.*, vol. 45, no. 3, pp. 450–460, May 2002.

[15] M. Thiel and D. Omeragic, "2D lateral imaging inversion for directional electromagnetic logging-while-drilling measurements," *Geophysics*, vol. 84, no. 6, pp. D217–D230, Nov. 2019.

[16] Y. Wang, "Gauss–Newton method," *Wiley Interdiscip. Rev. Comput. Stat.*, vol. 4, no. 4, pp. 415–420, Jul./Aug. 2012.

[17] Z. Wei and X. D. Chen, "Deep-learning schemes for full-wave nonlinear inverse scattering problems," *IEEE Trans. Geosci. Remote Sens.*, vol. 57, no. 4, pp. 1849–1860, Apr. 2019.

[18] A. Lucas, M. Iliadis, R. Molina, and A. K. Katsaggelos, "Using deep neural networks for inverse problems in imaging: Beyond analytical methods," *IEEE Signal Process. Mag.*, vol. 35, no. 1, pp. 20–36, Jan. 2018.

[19] J. Sun, Z. Niu, K. Innanen, J. Li, and D. Trad, "A theory-guided deep learning formulation of seismic waveform inversion," *Geophysics*, vol. 85, no. 2, pp. R87–R99, Jan. 2020.

[20] V. Puzyrev, "Deep learning electromagnetic inversion with convolutional neural networks," *Geophys. J. Int.*, vol. 218, no. 2, pp. 817–832, Aug. 2019.

[21] M. Shahriari, D. Pardo, A. Picon, A. Galdran, J. Del Ser, and C. Torres-Verdín, "A deep learning approach to the inversion of borehole resistivity measurements," *Comput. Geosci.*, vol. 24, no. 3, pp. 971–994, Apr. 2020.

[22] J. B. Fan, W. X. Zhang, W. X. Chen, and X. H. Li, "Inversion based on deep learning of logging-while-drilling directional resistivity measurements," *J. Petroleum Sci. Eng.*, vol. 208, Jan. 2022, Art. no. 109677.

[23] Y. Y. Hu, J. F. Chen, X. Q. Wu, and Y. Q. Huang, "A flexible and versatile joint inversion framework using deep learning," in *Proc. SEG/AAPG Int. Meeting Appl. Geosci. Energy*, Aug. 2022, pp. 1491–1495.

[24] G. Y. Zhu, M. Z. Gao, F. M. Kong, and K. Li, "A fast inversion of induction logging data in anisotropic formation based on deep learning," *IEEE Geosci. Remote Sens. Lett.*, vol. 17, no. 12, pp. 2050–2054, Dec. 2020.

[25] K. Noh, D. Pardo, and C. Torres-Verdin, "Deep-learning inversion method for the interpretation of noisy logging-while-drilling resistivity measurements," 2021, *arXiv:2111.07490*.

[26] K. Noh, D. Pardo, and C. Torres-Verdín, "2.5-D deep learning inversion of LWD and deep-sensing EM measurements across formations with dipping faults," *IEEE Geosci. Remote Sens. Lett.*, vol. 19, Nov. 2022, Art. no. 8023805.

[27] Y. C. Jin, Q. Y. Shen, X. Q. Wu, J. F. Chen, and Y. Q. Huang, "A physics-driven deep-learning network for solving nonlinear inverse problems," *Petrophysics*, vol. 61, no. 1, pp. 86–98, Feb. 2020.

[28] L. Zhang, "Application of neural networks to interpretation of well logs," *Spectrochim. Acta A, Mol. Biomol. Spectrosc.*, vol. 56, no. 5, pp. 1013–1020, 2000.

[29] J. Gao, C. H. Xu, and J. Q. Xiao, "Forward modelling of multi-component induction logging tools in layered anisotropic dipping formations," *J. Geophys. Eng.*, vol. 10, no. 5, Sep. 2013, Art. no. 054007.

[30] Y. Y. Hu, R. Guo, Y. C. Jin, X. Q. Wu, M. K. Li, A. Abubakar, and J. F. Chen, "A supervised descent learning technique for solving directional electromagnetic logging-while-drilling inverse problems," *IEEE Trans. Geosci. Remote Sens.*, vol. 58, no. 11, pp. 8013–8025, Nov. 2020.

[31] Y. L. Ao, W. K. Lu, Q. Y. Hou, and B. W. Jiang, "Sequence-to-sequence borehole formation property prediction via multi-task deep networks with sparse core calibration," *J. Petroleum Sci. Eng.*, vol. 208, Jan. 2022, Art. no. 109637.

[32] J. Brownlee, *Better Deep Learning: Train Faster, Reduce Overfitting, and Make Better Predictions*. Vermont, VIC, Australia: Machine Learning Mastery, 2018.

ZHENGMING KANG received the Ph.D. degree from the College of Geosciences, China University of Petroleum, Beijing, China, in 2019. Then, he joined Xi'an Shiyou University. His research consists of the theory, method, and basic application of resistivity logging tools. He accumulated a lot of experience in the forward and inversion of azimuth electromagnetic LWD measurements and LWD resistivity imaging tools. His current research interests include the design and optimization of new logging detectors and the forward and inverse of the LWD tool.

YI ZHANG received the B.S. degree in exploration technology and engineering and the M.S. degree in earth exploration and information technology from Jilin University, China, in 2009 and 2012, respectively, and the Ph.D. degree in mineral survey and exploration from the China Coal Research Institute, in 2022. From 2012 to 2019, he was a Logging Operator and a Logging Instruments Researcher with Shengli Logging Company, Sinopec. Since 2022, he has been engaged in the research and development of downhole drilling instruments with the Xi'an Research Institute, China Coal Technology and Engineering Group Corporation. His current research interest includes electromagnetic wave logging methods and instruments.

HAOJIE QIN received the B.S. degree from the College of Electrical Engineering, Henan University of Science and Technology, Luoyang, China, in 2021. He is currently pursuing the Graduate degree with Xi'an Shiyou University. His current research interests include the forward and inversion of azimuthal electromagnetic logging while drilling. As the second author, he has published three articles in this field.

WEI GAN received the B.S., M.S., and Ph.D. degrees from the School of Electronic Engineering, Xidian University, Xi'an, China, in 2007, 2009, and 2013, respectively. From April 2013 to November 2017, he was with the 20th Research Institute of CLP Group, mainly responsible for the research and development of land-based navigation. He transferred to the School of Electronic Engineering, Xi'an Shiyou University, in December 2017, where he has been engaged in the teaching and researching of measurement and control technology for a long time. He has completed eight national projects as the main participant and responsible person and published ten articles as the first author or corresponding author. His current research interests include information fusion, neural networks, navigation and positioning, and intelligent optimization.

GANG CHEN received the Ph.D. degree in geological resources and geological engineering from the China University of Petroleum, East China. He is currently with the Xian Research Institute, China Coal Technology and Engineering Group Corporation. He has been committed to the research of geosteering tools, rotary steerable tools, and the measurement of logging while drilling in coal mines for many years.